

# Beyond Backpropagation: Optimization with Multi-Tangent Forward Gradients

Katharina Flügel<sup>1,2</sup> Daniel Coquelin<sup>1,2</sup> Marie Weiel<sup>1,2</sup> Achim Streit<sup>1</sup> Markus Götz<sup>1,2</sup>

<sup>1</sup> Scientific Computing Center, Karlsruhe Institute of Technology

<sup>2</sup> Helmholtz AI

## Abstract

The gradients used to train neural networks are typically computed using backpropagation. While an efficient way to obtain exact gradients, backpropagation is computationally expensive, hinders parallelization, and is biologically implausible. Forward gradients are an approach to approximate the gradients from directional derivatives along random tangents computed by forward-mode automatic differentiation. So far, research has focused on using a single tangent per step. This paper provides an in-depth analysis of multi-tangent forward gradients and introduces an improved approach to combining the forward gradients from multiple tangents based on orthogonal projections. We demonstrate that increasing the number of tangents improves both approximation quality and optimization performance across various tasks.

## 1 INTRODUCTION

Neural networks are typically trained by minimizing a loss using gradient descent, that is, updating the network parameters by stepping in the opposite direction of their gradient. Backpropagation (Rumelhart et al., 1986; Linnainmaa, 1970) is widely used to compute these gradients efficiently and accurately but comes with several drawbacks. Taking about twice the time of the forward pass (Kaplan et al., 2020), it accounts for a large fraction of the training time, directly contributing to the consumed energy (Debus et al., 2023). Its forward-backward dependencies furthermore lead to suboptimal memory access patterns (Crafton et al., 2019) and hinder parallelization (Belilovsky et al., 2020). For example, when

pipelining the training over the network layers, these dependencies can lead to pipeline bubbles and underutilization (Narayanan et al., 2019; Huang et al., 2019). Besides these practical issues, backpropagation is incompatible with the biological motivation behind artificial neural networks, as biological neural networks lack such backward pathways to communicate update information (Bengio et al., 2016).

To overcome these issues, there has been much interest in alternative approaches to train neural networks. One promising approach, the recently proposed *forward gradient* (Baydin et al., 2022; Silver et al., 2022), uses forward-mode automatic differentiation to compute a directional derivative along a random tangent, approximating the gradient in a single forward pass. This method has shown great potential for training both fully-connected and convolutional neural networks. However, with increasing dimension, i.e., model parameter count, the approximation quality decreases while the variance of the forward gradient increases (Belouze, 2022; Ren et al., 2023). By sampling a random direction, the forward gradient acts as a Monte-Carlo approximation of the gradient. We thus expect that increasing the number of tangents will improve the approximation quality, enabling forward gradients to scale to larger dimensions and improving their robustness. Using multiple tangents has been previously mentioned (Baydin et al., 2022; Silver et al., 2022) but has not yet been analyzed in detail or evaluated experimentally.

In this work, we aim to fill this gap by taking a detailed look at how using multiple tangents can improve the forward gradient. Specifically, we aim to answer the following research questions:

- RQ1** Does using multiple tangents improve the forward gradient?
- RQ2** How should the forward gradient information from multiple tangents be combined?
- RQ3** Can multi-tangent forward gradients scale to state-of-the-art architectures?
- RQ4** What are the trade-offs of multiple tangents?

## 2 RELATED WORK

Our study builds upon previous research on forward gradients. Baydin et al. (2022) and Silver et al. (2022) introduce the forward gradient, an approach to approximate the gradient with the directional derivative along a random direction, resulting in an unbiased estimator of the gradient. A follow-up study by Belouze (2022) further analyzes the forward gradient on the Beale and Rosenbrock functions, revealing significant shortcomings in high dimensions. The author suggests sampling tangents from the Rademacher distribution to minimize the variance. Ren et al. (2023) show that the variance of the forward gradient estimation increases with the dimension and find that activity perturbation reduces this variance compared to weight perturbation. They use a custom architecture based on MLP Mixer (Tolstikhin et al., 2021) and combine activity perturbation with numerous local losses to scale up to ImageNet (Deng et al., 2009). Fournier et al. (2023) introduce a systematic framework to combine different gradient targets and gradient guesses, i.e., tangents. They observe significant improvements from using local update signals as tangents instead of random noise, scaling up to ResNet18 (He et al., 2016) and ImageNet32 (Chrabaszcz et al., 2017).

Besides forward gradients, numerous other approaches seek to train neural networks without backpropagation, often to overcome its biological implausibility. Feedback Alignment (Lillicrap et al., 2016) aims to enhance biological plausibility and solve the so-called weight transport problem (Grossberg, 1987) by communicating feedback signals backward along random, untrained feedback paths. Follow-up works (Nøkland, 2016; Frenkel et al., 2021; Flügel et al., 2023) replace this backward step with direct forward communication to each layer, effectively addressing the update locking problem (Jaderberg et al., 2017). Bacho and Chu (2024) combine direct feedback alignment (Nøkland, 2016) with forward gradients and momentum to reduce the gradient variance. The forward-forward algorithm (Hinton, 2022) trains neural networks using two forward passes—one on positive data and another on negative data—while applying local updates to differentiate between them. Similarly, PEPITA (Della-ferrera and Kreiman, 2022) applies a second forward pass on a randomly modulated input, which has been shown to be a special case of forward-forward (Srinivasan et al., 2024). Synthetic gradients (Jaderberg et al., 2017; Czarnecki et al., 2017) approximate the gradient by training layer-local models that predict the gradient using only local information, effectively decoupling the layers.

## 3 MULTI-TANGENT FORWARD GRADIENTS

### 3.1 Background

A typical neural network consists of *layers*  $l_1, \dots, l_L$ , each processing an input  $h_{i-1}$  from the previous layer, starting from the network input  $h_0$ , and passing the output  $h_i$  on to the next layer. Each layer depends on parameters  $\theta_i$ , which are adjusted during training. A layer can thus be seen as a function  $l_i : \Theta_i \times H_{i-1} \rightarrow H_i$ ,  $(\theta_i, h_{i-1}) \mapsto h_i$ , mapping the parameter space  $\Theta_i$  and the input space  $H_{i-1}$  to the output space  $H_i$ . In the *forward pass*, an input  $x = h_0$  is mapped to an output  $y = h_L$  by successively applying these layers. Using this layer definition, we can define the entire model as a function  $m : \Theta \times X \rightarrow Y$  with  $\Theta = \Theta_1 \times \dots \times \Theta_L$ ,  $X = H_0$ , and  $Y = H_L$ , where  $m(\theta, x) \mapsto l_L(\theta_L, l_{L-1}(\dots, l_1(\theta_1, x)))$  with  $\theta = (\theta_1, \dots, \theta_L)$ .

To train the model in a supervised fashion, we need an optimization metric, the *loss function*  $\mathcal{L} : Y \times Y \rightarrow \mathbb{R}$ , which measures how much the model output  $y = m(\theta, x)$  for input  $x$  differs from the corresponding target  $y^*$ . We then train the model by minimizing the loss  $\mathcal{L}(y, y^*)$ , i.e., minimizing the objective function  $f : \Theta \times X \times Y \rightarrow \mathbb{R}$ ,  $(\theta, x, y^*) \mapsto \mathcal{L}(m(\theta, x), y^*)$  for a set of input samples  $(x, y^*)$  by varying the parameters  $\theta$ . A common method to minimize such a function is *gradient descent*, where we take small steps in the opposite direction of the gradient

$$\nabla f(\theta, x, y^*) = \frac{\partial f(\theta, x, y^*)}{\partial \theta} \quad (1)$$

of  $f(\theta, x, y^*)$  with respect to the parameters  $\theta$ . During training, the parameters are iteratively updated as

$$\theta \leftarrow \theta - \eta \nabla f(\theta, x, y^*) \quad (2)$$

using a scalar learning rate  $\eta$ . More advanced optimizers like Adam (Kingma and Ba, 2015) introduce additional terms, such as momentum and parameter-wise adaptive learning rates, while retaining the core idea of computing the gradient and stepping in the opposite direction. Instead of using the exact gradient  $\nabla f$ , one can also train the model with an *approximate gradient*  $g$ , such as the forward gradient introduced in Section 3.2, by replacing  $\nabla f$  in Equation 2 with  $g$ .

Computing the gradient  $\nabla f$  is a non-trivial task. Multiple methods exist, for example, by analytically deriving a closed-form solution or numerically approximating the gradient using the finite differences approach. However, most are impractical for complex neural networks due to inefficient computation and numerical instability (Baydin et al., 2018). This is why automatic

differentiation, specifically backpropagation (Rumelhart et al., 1986; Linnainmaa, 1970), is commonly used to compute gradients for neural network training.

*Automatic differentiation (AD)* is a computationally efficient approach for computing partial derivatives by repeatedly applying the chain rule and simplifying intermediate results to numerical values. The objective function  $f(\theta, x, y^*)$  is a function composition whose derivative can be calculated using the chain rule. As an example, let us consider a function composition  $f : \mathbb{R} \rightarrow \mathbb{R}, x \mapsto g_3(g_2(g_1(x)))$  with  $g_i : \mathbb{R} \rightarrow \mathbb{R}$  and let  $h_i = (g_i \circ \dots \circ g_1)(x)$ . The derivative of  $y = f(x)$  with respect to  $x$  is

$$\frac{\partial y}{\partial x} = \frac{\partial y}{\partial h_2} \frac{\partial h_2}{\partial h_1} \frac{\partial h_1}{\partial x}. \quad (3)$$

This product can be computed starting from either end, resulting in a forward- and a reverse-mode of AD. The forward-mode initializes  $\partial x/\partial x = 1$  and successively computes  $\partial h_i/\partial x$  from  $\partial h_{i-1}/\partial x$ , while reverse-mode AD initializes  $\partial y/\partial y = 1$  and computes  $\partial y/\partial h_i$  from  $\partial y/\partial h_{i+1}$ . Higher dimensions are more complex as the derivative of a function  $f : \mathbb{R}^n \rightarrow \mathbb{R}^m, x \mapsto (f_1(x), \dots, f_m(x))$  is the  $m \times n$  Jacobi matrix  $\mathbf{J}_f$ . To compute all entries of  $\mathbf{J}_f$ , forward-mode requires  $n$  passes, as it needs to initialize  $n$  different  $\partial x/\partial x$  for all  $n$  dimensions of  $x$ . This corresponds to computing the Jacobi-vector product  $\mathbf{J}_f v$  for  $v \in \mathbb{R}^n$ . Correspondingly, reverse-mode requires  $m$  passes with different  $\partial y/\partial y$ , each computing the vector-Jacobi product  $v^\top \mathbf{J}_f$  for a  $v \in \mathbb{R}^m$ .

The time complexity of evaluating  $f$  and computing  $k$  passes in either forward- or reverse-mode is  $\omega \cdot \text{ops}(f)$ , where  $\text{ops}(f)$  is the time required for evaluating  $f$  (inference), with  $\omega \leq 1 + 1.5k$  for forward-mode and  $\omega \leq 1.5 + 2.5k$  for reverse-mode AD (Griewank and Walther, 2008). As obtaining the full Jacobi matrix  $\mathbf{J}_f$  requires  $k = n$  forward-mode or  $k = m$  reverse-mode passes, the decision between them depends on the dimensions  $n$  and  $m$ . When training a neural network with many parameters (large  $n$ ) by minimizing a scalar loss ( $m = 1$ ), computing the exact gradient  $\nabla f$  is much more efficient with reverse-mode AD than forward-mode AD. The special case of reverse-mode AD for  $m = 1$  is also known as *backpropagation (BP)*.

While backpropagation is more efficient than forward-mode AD for computing exact high-dimensional gradients  $\nabla f$ , it comes with several drawbacks, such as forward, update, and backward locking (Jaderberg et al., 2017), which limit both its biological plausibility and the potential for model parallelism and pipelining. An alternative to computing exact gradients in reverse-mode is computing approximate gradients based on forward computation.

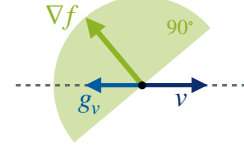


Figure 1: The forward gradient  $g_v$  for the tangent  $v$  is a projection of the gradient  $\nabla f$  on the (1D) subspace spanned by  $v$ . It is by definition always within  $90^\circ$  of  $\nabla f$  and thus a descending direction of  $f$ .

### 3.2 Forward Gradient

The *forward gradient* (Baydin et al., 2022; Silver et al., 2022) is an approach to approximate the gradient  $\nabla f$  using the directional derivative  $\partial f/\partial v = \nabla f \cdot v$  along a tangent  $v \in \mathbb{R}^n$ , and multiplying it with the tangent  $v$ . This directional derivative can be computed efficiently in a single forward-mode AD pass.

**Definition 1** (Forward Gradient). The forward gradient  $g_v$  for a tangent  $v \in \mathbb{R}^n$  is defined as

$$g_v = (\nabla f \cdot v)v. \quad (4)$$

The forward gradient has multiple useful properties.

**Property 1** (Unbiased Estimator). The forward gradient  $g_v$  is an unbiased estimator of  $\nabla f$ , i.e.,  $\mathbb{E}[g_v] = \nabla f$ , when sampling the tangent  $v$  randomly with iid. entries  $[v]_i$  with zero mean and unit variance (Baydin et al., 2022; Silver et al., 2022).

**Property 2** (Within  $90^\circ$ ). The forward gradient  $g_v$  is within  $90^\circ$  of  $\nabla f$  for any tangent  $v$  if  $g_v \neq 0$ .

*Proof.* The dot-product of  $g_v \neq 0$  and  $\nabla f$  is positive

$$g_v \cdot \nabla f = (\nabla f \cdot v)(v \cdot \nabla f) = (\nabla f \cdot v)^2 \geq 0, \quad (5)$$

and thus their angle is between  $0^\circ$  and  $90^\circ$ .  $\square$

**Property 3** (Descending Direction). The forward gradient is always a descending direction of  $f$  (Silver et al., 2022). This follows directly from Property 2.

**Property 4.** The forward gradient maps  $\nabla f$  from  $\mathbb{R}^n$  onto the one-dimensional subspace spanned by  $v \neq 0$ . If  $v$  is a unit vector,  $g_v$  is a projection.

Property 4 follows directly from Definition 1 and is illustrated in Figure 1. Besides these beneficial properties, there are several drawbacks to consider. While the forward gradient  $g_v$  is an unbiased estimator, it suffers from a high variance that increases with the number of parameters  $n$  (Belouze, 2022; Ren et al., 2023), thus reducing the accuracy of the gradient approximation. To measure the approximation quality, we can decompose the difference between  $g_v$  and  $\nabla f$

into the angle  $\gamma$  between them, measured by the cosine similarity

$$S_C(\nabla f, g_v) = \cos(\gamma) = \frac{\nabla f \cdot g_v}{\|\nabla f\|_2 \|g_v\|_2} \quad (6)$$

and the ratio of their vector lengths

$$\frac{\|g_v\|_2}{\|\nabla f\|_2}. \quad (7)$$

**Property 5** (Cosine Similarity). The cosine similarity for  $v \sim \mathcal{N}(0, I_n)$  decreases with  $n$  and approaches

$$\mathbb{E}[S_C(\nabla f, g_v)] = \sqrt{\frac{2}{\pi n}}. \quad (8)$$

For large  $n$ , this approaches zero, i.e., orthogonality.

**Property 6** (Magnitude). The magnitude of  $g_v$  for  $v \sim \mathcal{N}(0, I_n)$  increases with  $n$  and approaches

$$\mathbb{E}\left[\frac{\|g_v\|_2}{\|\nabla f\|_2}\right] = \sqrt{\frac{2n}{\pi}}. \quad (9)$$

Proofs for Properties 5 and 6 are given in Appendix A.1. In summary, with increasing gradient dimension  $n$ , the forward gradient’s direction becomes less accurate while its magnitude increases simultaneously, resulting in larger steps being taken in worse directions. We confirm this observation experimentally in Section 4 and find that with increasing  $n$ , the single-tangent forward gradient struggles to optimize even trivial functions like the *Sphere* function.

### 3.3 Multi-Tangent Forward Gradients

When sampling tangents randomly,  $g_v$  acts as a Monte-Carlo approximation of  $\nabla f$ . Consequently, we expect the approximation quality to improve with more samples, leading us to the definition of a multi-tangent forward gradient (**RQ1**).

**Definition 2** (Multi-Tangent Forward Gradient). The multi-tangent forward gradient  $g_V$  over a set of  $k$  tangents  $V = \{v_1, \dots, v_k\}$ ,  $v_i \in \mathbb{R}^n$  is defined as

$$g_V = \bigoplus_{v_i \in V} g_{v_i} \quad (10)$$

for an aggregation operator  $\oplus$ .

**Lemma 1.** Let  $V = \{v_1, \dots, v_k\}$  be  $k$  linearly independent tangents  $v_i \in \mathbb{R}^n$  and  $U = \text{span}(V) \subseteq \mathbb{R}^n$  the  $k$ -dimensional subspace spanned by  $V$ . For any linear combination  $\oplus$  applies  $g_V \in U$ .

A key question is how to combine the single-tangent forward gradients  $g_{v_1}, \dots, g_{v_k}$  into a multi-tangent forward gradient, i.e., how to choose  $\oplus$  (**RQ2**). Two approaches have been suggested so far:

**Definition 3.** The multi-tangent forward gradient as a sum (Baydin et al., 2022) is defined as

$$g_V^+ = \sum_{i=1}^k g_{v_i} = \mathbf{V} \mathbf{V}^\top \nabla f \quad (11)$$

with  $\mathbf{V} = (v_1 | \dots | v_k)$ .

**Definition 4.** The multi-tangent forward gradient as average (Silver et al., 2022) is defined as

$$\overline{g_V} = \frac{1}{k} g_V^+. \quad (12)$$

They correspond to choosing  $\oplus = \sum$  and  $\oplus = \overline{\phantom{x}}$ , respectively. The resulting multi-tangent forward gradient differs only in its magnitude but not its direction, which is easily offset by the learning rate.

When using all  $n$  standard basis vectors  $e_1, \dots, e_n$  as tangents (i.e.,  $k = n$ ),  $g_V^+$  corresponds to computing the exact gradient with full forward-mode AD, computing  $\nabla f$  for one parameter at a time as described in Section 3.1. However, when sampling the tangents randomly, e.g.,  $v_i \sim \mathcal{N}(0, I_n)$ ,  $g_V^+$  does generally not equal  $\nabla f$ , even for  $k = n$  tangents, as shown in Section 4.1. This limitation arises from the aggregation method used to combine multiple forward gradients  $g_{v_i}$ : both average and sum are conical combinations, which restrict the result to the cone spanned by the  $g_{v_i}$  and, consequently, the tangents  $v_i$ , as  $g_{v_i}$  is always (anti-)parallel to  $v_i$ . Moreover, they ignore the approximation quality of the different  $g_{v_i}$  and their interrelations. That is why even when using  $k \geq n$  linearly independent tangents,  $g_V^+$  and  $\overline{g_V}$  may fail to perfectly approximate  $\nabla f$ , despite having sufficient information to reconstruct the entire gradient.

### 3.4 Improved Multi-Tangent Forward Gradients With Orthogonal Projection

To improve the resulting multi-tangent forward gradient, we aim to use all information available from the single-tangent forward gradients.

**Definition 5** (Forward Orthogonal Gradient). Let  $V = \{v_1, \dots, v_k\}$  be  $k$  linearly independent tangents with  $U = \text{span}(V)$  and  $\mathbf{V} = (v_1 | \dots | v_k)$ , then the *orthogonal projection* of  $\nabla f$  onto  $U$  is defined as

$$P_U(\nabla f) = \mathbf{V}(\mathbf{V}^\top \mathbf{V})^{-1} \mathbf{V}^\top \nabla f. \quad (13)$$

**Lemma 2.**  $P_U(\nabla f)$  is the most accurate approximation  $g$  of  $\nabla f$  in  $U$  and minimizes  $\|\nabla f - g\|_2$ .

Compared to  $g_V^+$  (Definition 3),  $P_U(\nabla f)$  uses the same vector of directional derivatives  $\mathbf{V}^\top \nabla f$  but “corrects”  $V$  to an orthonormal basis using the inverse Gram matrix  $G(V)^{-1} = (\mathbf{V}^\top \mathbf{V})^{-1}$  before aggregating it. The

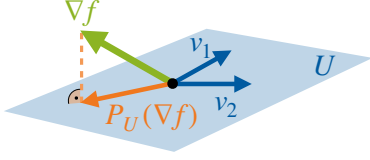


Figure 2: Orthogonal projection for  $n = 3$  and  $k = 2$ . The tangents  $v_1$  and  $v_2$  span a two-dimensional plane  $U$ . The gradient  $\nabla f$  does not lie within this plane, but its orthogonal projection  $P_U(\nabla f)$  provides the closest approximation of  $\nabla f$  in  $U$ .

orthogonal projection  $P_U(\nabla f)$  can thus be easily computed from the tangents’ directional derivatives, providing a new multi-tangent forward gradient with improved accuracy (**RQ2**). This is related to the geometrical interpretation given by Silver et al. (2022); however, rather than requiring  $V$  to be an orthonormal basis, our approach can handle arbitrary sets of linearly independent tangents. Figure 2 illustrates  $P_U(\nabla f)$  with a three-dimensional example.

Approximating  $\nabla f$  with  $P_U(\nabla f)$  solves two problems at once: the dependency of  $\|g_v\|_2$  on  $\|v\|_2$ , discussed in Section 3.2, and the suboptimal use of available information, outlined in Section 3.3. As a result,  $P_U(\nabla f)$  yields the true gradient for  $k = n$  linearly independent tangents and the best possible approximation for  $k < n$  tangents. Thus,  $P_U(\nabla f)$  is at least as accurate as the multi-tangent forward gradients  $g_V^+$  and  $\bar{g}_V$  introduced previously. Most importantly,  $P_U(\nabla f) = \nabla f$  when  $\nabla f \in U$ .

### 3.5 Time Complexity of Forward Gradients

Computing a  $k$ -tangent forward gradient  $g_V^+$  or  $\bar{g}_V$  has a time complexity of  $\mathcal{O}(k \cdot \text{ops}(f))$  and aligns with the complexity of  $k$  forward-mode AD passes (see Section 3.1). Constructing  $G(V)^{-1}$  for  $P_U(\nabla f)$  introduces an additional overhead of  $\mathcal{O}(k^2 n)$ , which is dominated by  $\mathcal{O}(k \cdot \text{ops}(f))$  when  $k$  is restricted to small constants, but must be considered for arbitrarily large  $k$ . A detailed derivation of these complexities is given in Appendix A.2. In both cases, the time complexity scales with  $k$ , which limits the applicability of multi-tangent forward gradients since there is only about a factor of two to gain over backpropagation (Kaplan et al., 2020), making any value of  $k$  beyond small constants rather impractical (**RQ4**). Despite the computational overhead, it is crucial to study the potential gain from multi-tangent forward gradients as the theoretical overhead may be partially offset by more efficient implementations, beneficial memory access patterns, and additional parallelization opportunities.

## 4 EVALUATION

We evaluate multi-tangent forward gradients in terms of their approximation quality and optimization performance. To highlight the differences between the gradients, we use stochastic gradient descent without momentum or learning rate schedule. We optimize multiple closed-form functions and train neural networks on the image classification datasets MNIST (Lecun et al., 1998) and CIFAR10 (Krizhevsky, 2009) using cross-entropy loss and activity perturbation. To adjust for the different gradient norms, we perform a learning rate search for each variant using Propulate (Taubert et al., 2023). More details are given in Appendix B. All experiments were conducted using an Intel Xeon Platinum 8368 processor and an NVIDIA A100-40 GPU and implemented in Python 3.9.16 using PyTorch (Paszke et al., 2019) 2.2.2 with CUDA 12.4. Our code is publicly available at [github.com/Helmholtz-AI-Energy/frog](https://github.com/Helmholtz-AI-Energy/frog).

### 4.1 Approximation Quality

First, we evaluate how well different forward gradients approximate the true gradient  $\nabla f$  by considering their difference in terms of direction, via the cosine similarity (Eq. 6), and magnitude, via the ratio of their norms (Eq. 7). We use a fixed gradient  $\nabla f = (1, \dots, 1)^\top \in \mathbb{R}^n$  and approximate it using the forward-gradient approaches introduced in Section 3: the single-tangent forward gradient  $g_v$  and multi-tangent forward gradients using either a sum ( $g_V^+$ ), an average ( $\bar{g}_V$ ), or the orthogonal projection ( $P_U$ ) for a set of  $k$  tangents  $V = \{v_1, \dots, v_k\}$ ,  $v_i \sim \mathcal{N}(0, I_n)$ . Additionally, we test sum and average with normalized tangents  $W = \{w_1, \dots, w_k\}$ ,  $w_i = v_i / \|v_i\|_2$ , labeled as  $g_W^+$  and  $\bar{g}_W$ , respectively. Due to the rotational invariance of  $\mathcal{N}(0, I_n)$ , the choice of  $\nabla f$  does not affect our results.

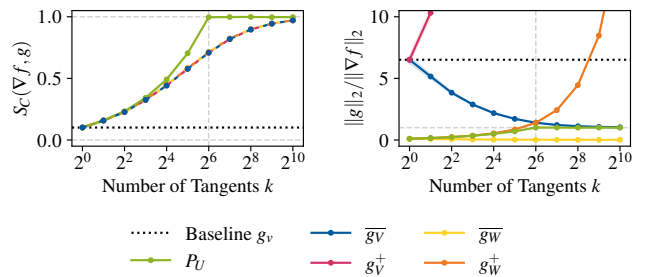


Figure 3: The approximation quality of different forward gradient approaches for  $n = 64$  in terms of cosine similarity and relative vector norm, mean over 1000 seeds. As the cosine similarity of the conical combinations is identical, we use dashed lines to better visualize the overlapping curves.

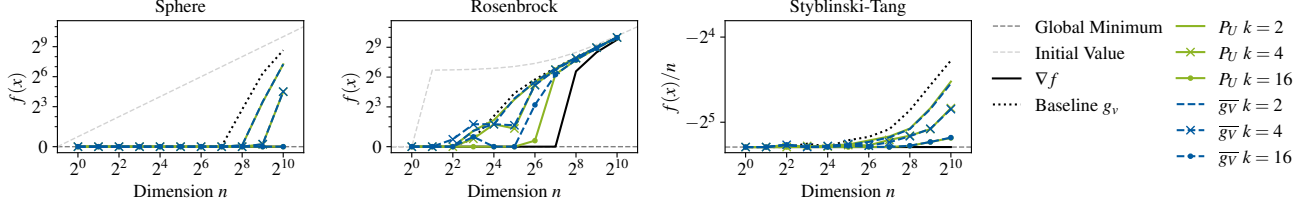


Figure 4: The best value found when minimizing  $f : \mathbb{R}^n \rightarrow \mathbb{R}$  with different gradient approximations, mean over five random seeds. To improve clarity for *Styblinski-Tang*, we plot  $f(x)/n$  instead, as the global minimum  $-39.17n$  scales with  $n$ , and cut off the initial value (0 for all  $n$ ) to zoom in on the relevant data.

Figure 3 illustrates our results for  $n = 64$  over 1000 seeds. The dashed vertical line marks  $k = 64 = n$ ; beyond this point, we could obtain a perfect approximation using full forward-mode AD. The single-tangent baseline  $g_v$  remains constant with  $k = 1$ . For the cosine similarity, we observe that all values lie between zero and one, confirming experimentally that the forward gradient is always within  $90^\circ$  as shown in Equation 5. As we increase the number of tangents, the cosine similarity increases, indicating a more accurate approximation of the true gradient’s direction. As expected, it is identical for all conical combinations  $g_V^+$ ,  $\bar{g}_V$ ,  $g_W^+$ , and  $\bar{g}_W$  and approaches one only for  $k \gg n$ . In contrast, the orthogonal projection  $P_U$  is exact for  $k \geq n$  and consistently outperforms the conical combinations, with the biggest gap around  $k \approx n$ .

The vector norm shows a notable difference between the conical combinations as sum  $(g_V^+, g_W^+)$  scales with  $k$  while averaging  $(\bar{g}_V, \bar{g}_W)$  over more tangents reduces the length. Moreover, the length of each forward gradient  $g_v$  scales with  $\|v\|_2^2$ . This is evident in our results, as the length using the non-normalized tangent set  $V$  scales with  $\mathbb{E}[\|v\|_2^2] = n$  compared to the normalized set  $W$ . For large  $k$ ,  $\bar{g}_V$  approaches the correct length. The orthogonal projection  $P_U$  performs similarly to  $g_W^+$  for small  $k$  but yields correct results for  $k \geq n$ , instead of significantly overestimating the gradient.

In summary, the orthogonal projection  $P_U$  matches or outperforms all conical combinations in terms of both direction and magnitude, with the largest difference around  $k \approx n$ . The conical combinations do not differ in their direction but only their length, which can be corrected by choosing an appropriate learning rate. That is why we consider only the mean of forward gradients for non-normalized tangents  $\bar{g}_V$  in the remaining experiments.

## 4.2 Optimizing Closed-Form Functions

We first evaluate the practical application of multi-tangent forward gradients by minimizing three classical, multidimensional, differentiable closed-form functions with gradient descent. While the strictly con-

vex *Sphere* function is straightforward to optimize, the *Rosenbrock* (Rosenbrock, 1960) and *Styblinski-Tang* functions (Styblinski and Tang, 1990) pose harder problems, with a long, narrow, flat valley around the global minimum and many local minima, respectively.

We evaluate the best value reached using different gradient approximations for increasing dimensions  $n$ , giving the mean over five random seeds in Figure 4. First, we observe that the single-tangent baseline  $g_v$  struggles to optimize even trivial functions like the *Sphere* for high-dimensional inputs. Adding more tangents consistently improves the optimization result, effectively extending the range at which the forward gradient achieves performance comparable to the true gradient  $\nabla f$ . The only exception is *Rosenbrock*, where we find that for small  $n$  and  $k$ , adding more tangents can actually decrease performance, especially for  $\bar{g}_V$ . Due to the complexity of optimizing *Rosenbrock*, where a few missteps can quickly lead to divergence, and the learning rate increasing with  $k$ ,  $\bar{g}_V$  can be more sensitive to the random seed.

Interestingly, the differences between  $\bar{g}_V$  and  $P_U$  are less pronounced than those observed in Section 4.1 when comparing the gradients themselves. For *Sphere* and *Styblinski-Tang*, they seem to have no impact on the final result. Only for *Rosenbrock* do we observe a notable improvement of  $P_U$  over  $\bar{g}_V$ , where  $P_U$  shows a more consistent improvement when adding more tangents. This might be due to the fact that tangents sampled from  $\mathcal{N}(0, I_n)$  are already very likely to be near orthogonal, limiting the potential impact of orthonormalization. On top of that, the difference in approximation quality observed in Section 4.1 between  $P_U$  and conical combinations is largest for  $k$  close to  $n$ . Yet the largest  $k$  tested here is  $k = 16$ , and for both *Sphere* and *Styblinski-Tang*, even the baseline  $g_v$  converges to the minimum for  $n \geq 16$ .

## 4.3 Non-Orthogonal Tangents

To investigate the benefits of orthogonal projection for arbitrary tangents, we study the behavior of  $P_U$  and  $\bar{g}_V$  with non-orthogonal tangents. For this, we con-



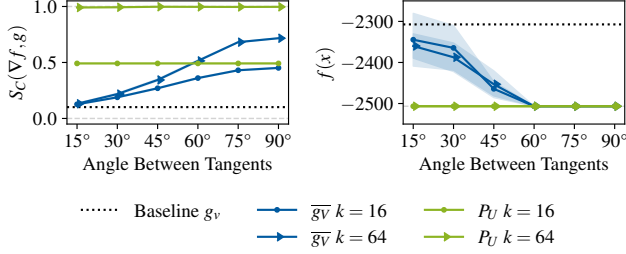


Figure 5: Cosine similarity (mean) and result on *Styblinski-Tang* with  $n = 64$  (mean and ci) for different tangent angles  $\alpha$  over 1000 and five seeds respectively.

construct a set of random tangents such that all tangents  $v_2, \dots, v_k$  have a fixed angle  $\alpha$  to the first tangent  $v_1$ . The first tangent is again sampled from  $\mathcal{N}(0, I_n)$ . All further tangents  $v_i$  are constructed by first sampling an  $u_i \sim \mathcal{N}(0, I_n)$  and then rotating  $u_i$  to  $v_i$  in the plane spanned by  $v_1$  and  $u_i$  such that the angle between  $v_i$  and  $v_1$  is  $\alpha$ . Intuitively, this samples the tangents randomly on an  $\alpha$ -cone around  $v_1$ . As we decrease  $\alpha$ , the cone narrows, causing all tangents to be closer to  $v_1$ .

Figure 5 gives the cosine similarity to  $\nabla f$  and the best result on *Styblinski-Tang*  $n = 64$  for different angles  $\alpha$ . As expected,  $P_U$  is entirely unaffected by  $\alpha$  as it implicitly orthonormalizes the tangents and thus only depends on the dimensionality of their spanned subspace but not their angle. In contrast,  $\overline{g_V}$  degrades as the cone around  $v_1$  narrows until it is barely an improvement over using a single tangent. This effect is more pronounced in the cosine similarity, where decreasing  $\alpha$  immediately reduces  $S_C(\nabla f, \overline{g_V})$ . In contrast, the optimization results on *Styblinski-Tang* continue to reach the optimum even down to  $60^\circ$ , with degradation only beginning for  $\alpha \leq 45^\circ$ . For  $\alpha = 90^\circ$ , the result is comparable to that obtained when using tangents sampled from  $\mathcal{N}(0, I_n)$  without rotation. This is in line with the expectation that such tangents are near-orthogonal.

#### 4.4 Fully-Connected Neural Networks

We transfer our results to neural networks by training a fully-connected network with two hidden layers and ReLU activations on MNIST using different forward gradient variants. We test three layer widths  $w = 256, 1024, 4096$  which correlate with the gradient dimension  $n$ . Figure 6 gives the best test error after training for each layer width and the test loss curves for  $w = 4096$ . As in the previous experiments, we observe a clear improvement from using more tangents, with  $k = 16$  achieving results close to the true gradient  $\nabla f$  despite  $k \ll n$ . We again find only little practical difference between  $P_U$  and  $\overline{g_V}$ , although  $P_U$  appears

more robust and results in slightly smoother training. Comparing different widths, we find that forward gradients can lose accuracy as the network size increases, whereas using  $\nabla f$  yields marginally better accuracy with larger  $w$ . This aligns with our previous observations that forward gradients with a fixed number of tangents become less accurate as we increase the input dimension  $n$ . The loss curves clearly show that all tested forward gradient approaches require significantly more epochs than  $\nabla f$ , which converges within 25 epochs. Using more tangents can both speed up the training process and improve the trained network’s predictive performance. However, it still takes significantly more epochs than using the true gradient  $\nabla f$  when both use appropriately tuned learning rates.

#### 4.5 Scaling to Larger Networks

To analyze the scalability of multi-tangent forward gradients (**RQ3**), we train a ResNet18 (He et al., 2016) and a small vision transformer (ViT) (Dosovitskiy et al., 2021) with six layers, four heads, 256 hidden dimensions, and 512 MLP dimensions on MNIST and CIFAR10. Table 1 states the minimum test errors after training with different gradient approximations. In line with our prior results, using more tangents reduces the test error, with  $k = 16$  achieving the best results among the tested forward gradients. Again, the distinction between the combination approaches is less clear and further complicated by the impact of the chosen learning rate since  $\overline{g_V}$  tends to be significantly larger than  $P_U$ , especially for small  $k$ . While this can, in theory, be corrected for, determining a suitable learning rate for such complex tasks is non-trivial. Suggesting the learning rate analytically to reduce the search space is thus an important avenue for further research. Overall, a significant gap between the forward gradients and the true gradient remains, in particular for more complex tasks. Combining multi-tangent forward gradients with better tangent sampling approaches appears to be a promising approach to further reduce this gap.

### 5 DISCUSSION

In this paper, we systematically investigate how using multiple tangents can improve forward gradients.

**Answer to RQ1: More tangents improve both gradient approximation and optimization.** Our results confirm prior assumptions that aggregating a forward gradient over multiple tangents improves its performance. Increasing the number of tangents  $k$  consistently improves both the approximation of the gradient’s direction (Section 4.1) and optimization perfor-

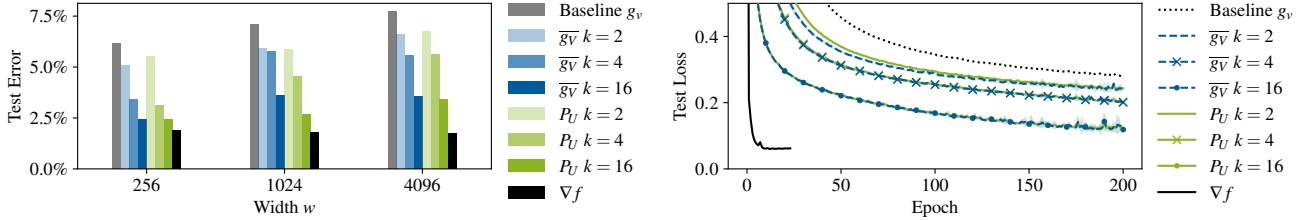


Figure 6: The best test error when training fully-connected networks with different hidden layer widths on MNIST and the test loss curve for width  $w = 4096$ . Mean over three seeds.

Table 1: Best test error in % after training with different (forward) gradients, mean over three seeds. Best value across forward gradients highlighted in bold.

|             |     | ResNet18    |              | VisionTransformer |              |
|-------------|-----|-------------|--------------|-------------------|--------------|
|             | $k$ | MNIST       | CIFAR10      | MNIST             | CIFAR10      |
| $\nabla f$  | –   | 0.68        | 47.29        | 2.36              | 46.38        |
| $g_v$       | 1   | 4.13        | 63.63        | 60.53             | 71.10        |
| $\bar{g}_V$ | 2   | 4.32        | 60.77        | 50.73             | 69.49        |
| $\bar{g}_V$ | 4   | 2.98        | 55.87        | 44.57             | 66.98        |
| $\bar{g}_V$ | 16  | 1.86        | 49.35        | <b>36.06</b>      | 63.68        |
| $P_U$       | 2   | 3.33        | 58.14        | 49.11             | 68.12        |
| $P_U$       | 4   | 3.14        | 55.24        | 44.08             | 65.72        |
| $P_U$       | 16  | <b>1.84</b> | <b>47.24</b> | 42.60             | <b>61.07</b> |

mance (Sections 4.2 to 4.5). We demonstrate that the single-tangent forward gradient often struggles in high-dimensional spaces, even for simple functions like the *Sphere*, consistent with prior observations (Belouze, 2022; Ren et al., 2023). By increasing  $k$ , we can alleviate this to a degree and scale to larger dimensions.

**Answer to RQ2: Orthogonal projection can yield more accurate forward gradients, especially for non-orthogonal tangents.** Our study of different combination approaches shows that the orthogonal projection of the gradient onto the subspace spanned by the tangents can be computed with low overhead from the individual forward gradients and yields the most accurate gradient approximation (Section 4.1). Somewhat surprisingly, this does not directly translate to better optimization performance; a simple average over the single-tangent forward gradients performs roughly on par with the orthogonal projection (Sections 4.2 to 4.5). We demonstrate that this is due to the tangent sampling method producing near-orthogonal tangents, which makes orthogonalization less impactful, and show that orthogonal projection significantly outperforms simpler combinations when one cannot rely on the tangents being near-orthogonal (Section 4.3).

**Answer to RQ3: Multi-tangent forward gradient can train ResNet18 and ViT.** In Section 4.5, we demonstrate that multi-tangent forward gradients can train residual networks and vision transformers, achieving significantly improved performance by using more tangents. Nonetheless, a considerable gap to the true gradient  $\nabla f$  remains. Combining multi-tangent forward gradients with better tangent sampling holds great promise for further improving these results.

**Answer to RQ4: Additional tangents are a trade-off between accuracy and compute.** As discussed in Section 3.5, the time complexity of forward gradients scales linearly with the number of tangents. From a theoretical perspective, we thus expect using any more than two tangents to result in a longer runtime than backpropagation. In practice, the more advantageous memory-access patterns of forward passes may allow an optimized implementation to compete with backpropagation, even for small  $k > 2$ . Yet, scaling  $k$  to  $\mathcal{O}(n)$  for large networks is unlikely to be feasible. However, our findings show that it is not necessary to scale  $k$  up to  $n$ ; even a few additional tangents can significantly enhance results.

**Outlook and Future Work** Multi-tangent forward gradients are largely independent of the gradient target and the tangents used, particularly when using orthogonal projection, as shown in Section 4.3. They can thus be easily integrated with approaches that replace the gradient target or tangents. By utilizing multiple tangents, we could even combine multiple different tangent sampling approaches to leverage the advantages of each. More advanced tangent sampling methods based on, e.g., local losses or auxiliary networks, may no longer be near orthogonal, thus benefiting further from orthogonal projection. We are excited about the potential of combining multi-tangent forward gradients with ongoing research in the field. Beyond that, it is highly promising to parallelize over the tangents, in addition to pipelining over the network layers enabled by the forward-only computation, as the forward passes per tangent are independent and yield a single scalar value for the directional derivative.



## Acknowledgements

This work is supported by the Helmholtz Association Initiative and Networking Fund on the HAICORE@KIT partition.

## References

- Bacho, F. and Chu, D. (2024). Low-variance Forward Gradients using Direct Feedback Alignment and momentum. *Neural Networks*, 169:572–583.
- Baydin, A. G., Pearlmutter, B. A., Radul, A. A., and Siskind, J. M. (2018). Automatic Differentiation in Machine Learning: a Survey. *Journal of Machine Learning Research*, 18(153):1–43.
- Baydin, A. G., Pearlmutter, B. A., Syme, D., Wood, F., and Torr, P. (2022). Gradients without Backpropagation. arXiv:2202.08587.
- Belilovsky, E., Eickenberg, M., and Oyallon, E. (2020). Decoupled Greedy Learning of CNNs. In *Proceedings of the 37th International Conference on Machine Learning*, pages 736–745. PMLR. ISSN: 2640-3498.
- Belouze, G. (2022). Optimization without Backpropagation. arXiv:2209.06302.
- Bengio, Y., Lee, D.-H., Bornschein, J., Mesnard, T., and Lin, Z. (2016). Towards Biologically Plausible Deep Learning. arXiv:1502.04156.
- Chrabaszcz, P., Loshchilov, I., and Hutter, F. (2017). A Downsampled Variant of ImageNet as an Alternative to the CIFAR datasets. arXiv:1707.08819.
- Crafton, B., West, M., Basnet, P., Vogel, E., and Raychowdhury, A. (2019). Local Learning in RRAM Neural Networks with Sparse Direct Feedback Alignment. In *2019 IEEE/ACM International Symposium on Low Power Electronics and Design (ISLPED)*, pages 1–6.
- Czarnecki, W. M., Świrszcz, G., Jaderberg, M., Osindero, S., Vinyals, O., and Kavukcuoglu, K. (2017). Understanding Synthetic Gradients and Decoupled Neural Interfaces. In *Proceedings of the 34th International Conference on Machine Learning*, pages 904–912. PMLR. ISSN: 2640-3498.
- Debus, C., Piraud, M., Streit, A., Theis, F., and Götz, M. (2023). Reporting electricity consumption is essential for sustainable AI. *Nature Machine Intelligence*, 5(11):1176–1178.
- Dellafrera, G. and Kreiman, G. (2022). Error-driven Input Modulation: Solving the Credit Assignment Problem without a Backward Pass. In *Proceedings of the 39th International Conference on Machine Learning*, pages 4937–4955. PMLR. ISSN: 2640-3498.
- Deng, J., Dong, W., Socher, R., Li, L.-J., Li, K., and Fei-Fei, L. (2009). ImageNet: A large-scale hierarchical image database. In *2009 IEEE Conference on Computer Vision and Pattern Recognition*, pages 248–255. ISSN: 1063-6919.
- Dosovitskiy, A., Beyer, L., Kolesnikov, A., Weissenborn, D., Zhai, X., Unterthiner, T., Dehghani, M., Minderer, M., Heigold, G., Gelly, S., Uszkoreit, J., and Houlsby, N. (2021). An Image is Worth 16x16 Words: Transformers for Image Recognition at Scale. In *International Conference on Learning Representations (ICLR)*.
- Flügel, K., Coquelin, D., Weiel, M., Debus, C., Streit, A., and Götz, M. (2023). Feed-Forward Optimization With Delayed Feedback for Neural Networks. arXiv:2304.13372.
- Fournier, L., Rivaud, S., Belilovsky, E., Eickenberg, M., and Oyallon, E. (2023). Can Forward Gradient Match Backpropagation? In *Proceedings of the 40th International Conference on Machine Learning*, pages 10249–10264. PMLR.
- Frenkel, C., Lefebvre, M., and Bol, D. (2021). Learning Without Feedback: Fixed Random Learning Signals Allow for Feedforward Training of Deep Neural Networks. *Frontiers in Neuroscience*, 15.
- Griewank, A. and Walther, A. (2008). *Evaluating Derivatives: Principles and Techniques of Algorithmic Differentiation*. Society for Industrial and Applied Mathematics, USA, second edition.
- Grossberg, S. (1987). Competitive learning: From interactive activation to adaptive resonance. *Cognitive Science*, 11(1):23–63.
- He, K., Zhang, X., Ren, S., and Sun, J. (2016). Deep residual learning for image recognition. In *Proceedings of the IEEE Conference on Computer Vision and Pattern Recognition (CVPR)*.
- Hinton, G. (2022). The Forward-Forward Algorithm: Some Preliminary Investigations. arXiv:2212.13345.
- Huang, Y., Cheng, Y., Bapna, A., Firat, O., Chen, D., Chen, M., Lee, H., Ngiam, J., Le, Q. V., Wu, Y., and Chen, Z. (2019). GPipe: Efficient Training of Giant Neural Networks using Pipeline Parallelism. In *Advances in Neural Information Processing Systems*, volume 32. Curran Associates, Inc.
- Jaderberg, M., Czarnecki, W. M., Osindero, S., Vinyals, O., Graves, A., Silver, D., and Kavukcuoglu, K. (2017). Decoupled Neural Interfaces using Synthetic Gradients. In *Proceedings of the 34th International Conference on Machine Learning*, pages 1627–1635. PMLR. ISSN: 2640-3498.

- Kaplan, J., McCandlish, S., Henighan, T., Brown, T. B., Chess, B., Child, R., Gray, S., Radford, A., Wu, J., and Amodei, D. (2020). Scaling Laws for Neural Language Models. arXiv:2001.08361.
- Kingma, D. P. and Ba, J. (2015). Adam: A Method for Stochastic Optimization. In Bengio, Y. and LeCun, Y., editors, *International Conference on Learning Representations (ICLR)*.
- Krizhevsky, A. (2009). Learning Multiple Layers of Features from Tiny Images. Technical report.
- Lankham, I., Nachtergaele, B., and Schilling, A. (2016). *Linear Algebra as an Introduction to Abstract Mathematics*. World Scientific.
- Lecun, Y., Bottou, L., Bengio, Y., and Haffner, P. (1998). Gradient-based learning applied to document recognition. *Proceedings of the IEEE*, 86(11):2278–2324.
- Lillicrap, T. P., Cownden, D., Tweed, D. B., and Akerman, C. J. (2016). Random synaptic feedback weights support error backpropagation for deep learning. *Nature Communications*, 7(1):13276.
- Linnainmaa, S. (1970). The representation of the cumulative rounding error of an algorithm as a Taylor expansion of the local rounding errors. *Master’s Thesis (in Finnish)*, Univ. Helsinki.
- Narayanan, D., Harlap, A., Phanishayee, A., Seshadri, V., Devanur, N. R., Ganger, G. R., Gibbons, P. B., and Zaharia, M. (2019). PipeDream: generalized pipeline parallelism for DNN training. In *Proceedings of the 27th ACM Symposium on Operating Systems Principles*, pages 1–15, Huntsville Ontario Canada. ACM.
- Nøkland, A. (2016). Direct feedback alignment provides learning in deep neural networks. In *Proceedings of the 30th International Conference on Neural Information Processing Systems*, pages 1045–1053, Red Hook, NY, USA. Curran Associates Inc.
- Paszke, A., Gross, S., Massa, F., Lerer, A., Bradbury, J., Chanan, G., Killeen, T., Lin, Z., Gimelshein, N., Antiga, L., Desmaison, A., Kopf, A., Yang, E., DeVito, Z., Raison, M., Tejani, A., Chilamkurthy, S., Steiner, B., Fang, L., Bai, J., and Chintala, S. (2019). PyTorch: An Imperative Style, High-Performance Deep Learning Library. In *Advances in Neural Information Processing Systems*, volume 32. Curran Associates, Inc.
- Ren, M., Kornblith, S., Liao, R., and Hinton, G. (2023). Scaling forward gradient with local losses. In *International Conference on Learning Representations (ICLR)*.
- Rosenbrock, H. H. (1960). An Automatic Method for Finding the Greatest or Least Value of a Function. *The Computer Journal*, 3(3):175–184.
- Rumelhart, D. E., Hinton, G. E., and Williams, R. J. (1986). Learning representations by back-propagating errors. *Nature*, 323(6088):533–536.
- Silver, D., Goyal, A., Danihelka, I., Hessel, M., and van Hasselt, H. (2022). Learning by directional gradient descent. In *International Conference on Learning Representations (ICLR)*.
- Srinivasan, R., Mignacco, F., Sorbaro, M., Refinetti, M., Cooper, A., Kreiman, G., and Dellaferrera, G. (2024). Forward learning with top-down feedback: Empirical and analytical characterization. arXiv:2302.05440.
- Styblinski, M. A. and Tang, T. S. (1990). Experiments in nonconvex optimization: Stochastic approximation with function smoothing and simulated annealing. *Neural Networks*, 3(4):467–483.
- Taubert, O., Weiel, M., Coquelin, D., Farshian, A., Debus, C., Schug, A., Streit, A., and Götz, M. (2023). Massively parallel genetic optimization through asynchronous propagation of populations. In *International Conference on High Performance Computing*, pages 106–124. Springer.
- Tolstikhin, I. O., Houlsby, N., Kolesnikov, A., Beyer, L., Zhai, X., Unterthiner, T., Yung, J., Steiner, A., Keysers, D., Uszkoreit, J., Lucic, M., and Dosovitskiy, A. (2021). MLP-Mixer: An all-MLP Architecture for Vision. In *Advances in Neural Information Processing Systems*, volume 34, pages 24261–24272. Curran Associates, Inc.

## A THEORETICAL RESULTS AND PROOFS

### A.1 Additional Proofs for Section 3

**Property 2** (Within  $90^\circ$ ). The forward gradient  $g_v$  is within  $90^\circ$  of  $\nabla f$  for any tangent  $v$  if  $g_v \neq 0$ .

*Proof.* The dot-product of  $g_v$  and  $\nabla f$  is positive

$$g_v \cdot \nabla f = ((\nabla f \cdot v)v) \cdot \nabla f = (\nabla f \cdot v)(v \cdot \nabla f) = (\nabla f \cdot v)^2 \geq 0. \quad (14)$$

If  $g_v \neq 0$  then  $\nabla f$  must also be non-zero as otherwise  $\nabla f \cdot v = 0$  and thus  $g_v = 0$ . Hence, for  $g_v \neq 0$  the gradient norms are strictly positive:  $\|g_v\|_2 > 0$  and  $\|\nabla f\|_2 > 0$ . It follows that the cosine similarity of  $g_v$  and  $\nabla f$  is positive

$$\cos(\gamma) = S_C(\nabla f, g_v) = \frac{g_v \cdot \nabla f}{\|g_v\|_2 \|\nabla f\|_2} \geq 0 \quad (15)$$

consequently

$$0 \leq \gamma = \arccos(\cos(\gamma)) \leq \frac{\pi}{2}. \quad (16)$$

The angle  $\gamma$  between  $g_v$  and  $\nabla f$  is thus between  $0^\circ$  and  $90^\circ$ .  $\square$

**Property 4.** The forward gradient  $g_v$  maps  $\nabla f$  from  $\mathbb{R}^n$  onto the one-dimensional subspace spanned by  $v \neq 0$ . If  $v$  is a unit vector,  $g_v$  is a projection.

*Proof.* Per Definition 1,

$$g_v = (\nabla f \cdot v)v \quad (17)$$

where the directional derivative  $\nabla f \cdot v$  is a scalar and  $v \in \text{span}\{v\}$ . Thus,  $g_v \in \text{span}\{v\}$ . If  $v$  is a unit vector, e.g.,  $\|v\|_2 = 1$ ,  $g_v$  is a projection:

$$(g_v \cdot v)v = ((\nabla f \cdot v)v \cdot v)v = (\nabla f \cdot v) \underbrace{(v \cdot v)}_{=1} v = (\nabla f \cdot v)v = g_v. \quad (18)$$

$\square$

**Proposition 1.** The normalized dot-product  $S_C(x, v)$  for a vector  $x \in \mathbb{R}^n$ ,  $n > 2$  and a random vector  $v \sim \mathcal{N}(0, I_n)$  has expectation zero, variance  $\frac{1}{n-2}$  and approaches the normal distribution  $\mathcal{N}(0, \frac{1}{n})$  for large  $n$ .

*Proof.* Since  $\mathcal{N}(0, I_n)$  is rotation invariant, i.e., every direction has the same probability, the distribution of angles to  $v \sim \mathcal{N}(0, I_n)$  is the same for any vector  $x \neq 0$  and the norm  $\|v\|_2$  is independent of the direction  $\frac{v}{\|v\|_2}$ . Let us therefore consider  $x = (1, \dots, 1)^\top$  with  $\|x\|_2 = \sqrt{n}$ . Let further  $[v]_i$  be the  $i$ -th entry of  $v$  and since  $v \sim \mathcal{N}(0, I_n)$ , the marginal distributions  $[v]_i$  are iid with  $[v]_i \sim \mathcal{N}(0, 1)$ . Then

$$S_C(x, v) = \frac{x \cdot v}{\|x\|_2 \|v\|_2} = \frac{\sum_{i=1}^n [v]_i}{\sqrt{n} \|v\|_2} \quad (19)$$

with

$$\mathbb{E}[S_C(x, v)] = \mathbb{E}\left[\frac{\sum_{i=1}^n [v]_i}{\sqrt{n} \|v\|_2}\right] = \frac{1}{\sqrt{n}} \mathbb{E}\left[\frac{1}{\|v\|_2}\right] \mathbb{E}\left[\sum_{i=1}^n [v]_i\right] = \frac{1}{\sqrt{n}} \mathbb{E}\left[\frac{1}{\|v\|_2}\right] \sum_{i=1}^n \underbrace{\mathbb{E}[[v]_i]}_{=0} = 0 \quad (20)$$

and

$$\text{Var}(S_C(x, v)) = \mathbb{E} \left[ \left( S_C(x, v) - \underbrace{\mathbb{E}[S_C(x, v)]}_{=0} \right)^2 \right] = \mathbb{E}[S_C(x, v)^2] \quad (21)$$

$$= \mathbb{E} \left[ \left( \frac{\sum_{i=1}^n [v]_i}{\sqrt{n} \|v\|_2} \right)^2 \right] = \mathbb{E} \left[ \frac{(\sum_{i=1}^n [v]_i)^2}{n \|v\|_2^2} \right] = \frac{1}{n} \mathbb{E} \left[ \frac{1}{\|v\|_2^2} \right] \mathbb{E} \left[ \left( \sum_{i=1}^n [v]_i \right)^2 \right] \quad (22)$$

$$= \frac{1}{n} \mathbb{E} \left[ \frac{1}{\|v\|_2^2} \right] \mathbb{E} \left[ \sum_{i=1}^n [v]_i^2 + 2 \sum_{i=1}^n \sum_{j=1}^{i-1} [v]_i [v]_j \right] \quad (23)$$

$$= \frac{1}{n} \mathbb{E} \left[ \frac{1}{\|v\|_2^2} \right] \left( \sum_{i=1}^n \underbrace{\mathbb{E}[v]_i^2}_{=1} + 2 \sum_{i=1}^n \sum_{j=1}^{i-1} \underbrace{\mathbb{E}[[v]_i [v]_j]}_{=0} \right) \quad (24)$$

$$= \frac{1}{n} \mathbb{E} \left[ \frac{1}{\|v\|_2^2} \right] \left( \sum_{i=1}^n 1 + 2 \sum_{i=1}^n \sum_{j=1}^{i-1} 0 \right) \quad (25)$$

$$= \frac{1}{n} \mathbb{E} \left[ \frac{1}{\|v\|_2^2} \right] n = \mathbb{E} \left[ \frac{1}{\|v\|_2^2} \right] = \frac{1}{n-2} \quad (26)$$

for  $n > 2$  since  $\|v\|_2^2 \sim \chi^2(n)$  and its inverse  $\frac{1}{\|v\|_2^2}$  thus follows the Inverse- $\chi^2$ -Distribution  $\text{Inv-}\chi^2(n)$ , i.e.,  $\frac{1}{\|v\|_2^2} \sim \text{Inv-}\chi^2(n)$  with mean  $\mathbb{E} \left[ \frac{1}{\|v\|_2^2} \right] = \frac{1}{n-2}$  for  $n > 2$ .

Furthermore, the central limit theorem states that  $\frac{1}{n} \sum_{i=1}^n X_i$  with iid samples  $X_i$  drawn from a distribution with expected value  $\mu$  and finite positive variance  $\sigma^2$  converges to the normal distribution  $\mathcal{N} \left( \mu, \frac{\sigma^2}{n} \right)$  for large  $n$ . Let  $X_i = \frac{\sqrt{n}[v]_i}{\|v\|_2}$  for  $v_i \sim \mathcal{N}(0, 1)$  with

$$\mu = \mathbb{E}[X_i] = \mathbb{E} \left[ \frac{\sqrt{n}[v]_i}{\|v\|_2} \right] = \sqrt{n} \mathbb{E} \left[ \frac{1}{\|v\|_2} \right] \underbrace{\mathbb{E}[[v]_i]}_{=0} = 0 \quad (27)$$

and

$$\sigma^2 = \text{Var}(X_i) = \text{Var} \left( \frac{\sqrt{n}[v]_i}{\|v\|_2} \right) = \mathbb{E} \left[ \left( \frac{\sqrt{n}[v]_i}{\|v\|_2} - 0 \right)^2 \right] \quad (28)$$

$$= \mathbb{E} \left[ \frac{n[v]_i^2}{\|v\|_2^2} \right] = n \mathbb{E} \left[ \frac{1}{\|v\|_2^2} \right] \mathbb{E}[[v]_i^2] = n \cdot \frac{1}{n-2} \cdot 1 = \frac{n}{n-2} \quad (29)$$

which approaches 1 for large  $n$ . Then

$$\frac{1}{n} \sum_{i=1}^n X_i = \frac{1}{n} \sum_{i=1}^n \frac{\sqrt{n}[v]_i}{\|v\|_2} = \frac{\sqrt{n}}{n} \sum_{i=1}^n \frac{[v]_i}{\|v\|_2} = \frac{\sum_{i=1}^n [v]_i}{\sqrt{n} \|v\|_2} = S_C(x, v) \quad (30)$$

approaches the normal distribution  $\mathcal{N} \left( 0, \frac{1}{n} \right)$  for large  $n$ .

□

**Property 5** (Cosine Similarity). The cosine similarity for  $v \sim \mathcal{N}(0, I_n)$  decreases with  $n$  and approaches

$$\mathbb{E}[S_C(\nabla f, g_v)] = \sqrt{\frac{2}{\pi n}}. \quad (31)$$

*Proof.* The cosine similarity of  $\nabla f$  and  $g_v$  corresponds to the absolute cosine similarity of  $\nabla f$  and  $v$

$$S_C(\nabla f, g_v) = \frac{\nabla f \cdot g_v}{\|\nabla f\|_2 \|g_v\|_2} = \frac{\nabla f \cdot (\nabla f \cdot v)v}{\|\nabla f\|_2 \|(\nabla f \cdot v)v\|_2} = \frac{(\nabla f \cdot v)^2}{\|\nabla f\|_2 \|\nabla f \cdot v\| \|v\|_2} = \frac{|\nabla f \cdot v|}{\|\nabla f\|_2 \|v\|_2} = |S_C(\nabla f, v)|. \quad (32)$$

This is no surprise since the forward gradient  $g_v$  is (anti-)parallel to the tangent  $v$ . Per Proposition 1,  $S_C(\nabla f, v)$  approaches  $\mathcal{N}(0, \frac{1}{n})$  for large  $n$  and thus  $S_C(\nabla f, g_v) = |S_C(\nabla f, v)|$  approaches the half-normal distribution with

$$\mathbb{E}[S_C(\nabla f, g_v)] = \mathbb{E}[|S_C(\nabla f, v)|] = \frac{\sigma\sqrt{2}}{\sqrt{\pi}} = \sqrt{\frac{2}{\pi n}}. \quad (33)$$

□

**Property 6** (Magnitude). The magnitude of  $g_v$  for  $v \sim \mathcal{N}(0, I_n)$  increases with  $n$  and approaches

$$\mathbb{E}\left[\frac{\|g_v\|_2}{\|\nabla f\|_2}\right] = \sqrt{\frac{2n}{\pi}}. \quad (34)$$

*Proof.* The magnitude of the forward gradient  $g_v$  is

$$\|g_v\|_2 = \|(\nabla f \cdot v)v\|_2 = \|\nabla f \cdot v\|_2 \|v\|_2 = \|\nabla f\|_2 \|v\|_2^2 \frac{|\nabla f \cdot v|}{\|\nabla f\|_2 \|v\|_2} = \|\nabla f\|_2 \|v\|_2^2 |S_C(\nabla f, v)| \quad (35)$$

and thus the ratio to the true gradient is

$$\frac{\|g_v\|_2}{\|\nabla f\|_2} = \frac{\|\nabla f\|_2 \|v\|_2^2 |S_C(\nabla f, v)|}{\|\nabla f\|_2} = \|v\|_2^2 |S_C(\nabla f, v)|. \quad (36)$$

As before,  $\|v\|_2^2 \sim \chi^2(n)$  with  $\mathbb{E}[\|v\|_2] = n$  and  $|S_C(\nabla f, v)|$  approaches the half-normal distribution for  $\mu = 0$  and  $\sigma^2 = \frac{1}{n}$  with  $\mathbb{E}[|S_C(\nabla f, v)|] = \sqrt{\frac{2}{\pi n}}$ . Since  $\mathcal{N}(0, I_n)$  is rotation invariant,  $\|v\|_2^2$  and  $|S_C(\nabla f, v)|$  are independent. Overall, it follows for large  $n$

$$\mathbb{E}\left[\frac{\|g_v\|_2}{\|\nabla f\|_2}\right] = \mathbb{E}[\|v\|_2^2 |S_C(\nabla f, v)|] = \mathbb{E}[\|v\|_2^2] \cdot \mathbb{E}[|S_C(\nabla f, v)|] = n \cdot \sqrt{\frac{2}{\pi n}} = \sqrt{\frac{2n}{\pi}}. \quad (37)$$

□

**Lemma 3.** Let  $V = \{v_1, \dots, v_k\}$  be  $k$  linearly independent tangents  $v_i \in \mathbb{R}^n$  and  $U = \text{span}(V) \subseteq \mathbb{R}^n$  the  $k$ -dimensional subspace spanned by  $V$ . For any linear combination  $\oplus$  applies  $g_V \in U$ .

Note that  $g_V$  here refers to a general multi-tangent forward gradient over the set of tangents  $V$ ;  $g_V^+$ ,  $\overline{g_V}$ ,  $P_U(\nabla f)$  are special cases of  $g_V$ .

*Proof.* Per Property 4, each single-tangent forward gradient  $g_{v_i}$  lies in  $\text{span}(\{v_i\}) \subseteq U$ . Thus, all  $g_{v_i}$  are in  $U$ . Per the definition of vector spaces, all linear combinations of vectors in  $U$  remain in  $U$  (closed under vector addition and scalar multiplication). Thus,  $g_V \in U$  for any linear combination  $\oplus$ . □

**Lemma 4.**  $P_U(\nabla f)$  is the most accurate approximation  $g$  of  $\nabla f$  in  $U$  and minimizes  $\|\nabla f - g\|_2$ .

Here,  $g$  refers to an arbitrary  $g \in U$ , including but not limited to, a forward gradient with tangents in  $U$ .

*Proof.* Based on the proof of Proposition 9.6.6 in Lankham et al. (2016), we show that

$$\|\nabla f - P_U(\nabla f)\|_2 \leq \|\nabla f - g\|_2 \quad (38)$$

for every  $g \in U$ . Let  $g \in U$ , then

$$\|\nabla f - P_U(\nabla f)\|_2^2 \leq \|\nabla f - P_U(\nabla f)\|_2^2 + \|P_U(\nabla f) - g\|_2^2 \quad \text{since } \|P_U(\nabla f) - g\|_2^2 \geq 0 \quad (39)$$

$$\leq \|\nabla f - P_U(\nabla f) + P_U(\nabla f) - g\|_2^2 \quad \text{with Pythagorean Theorem} \quad (40)$$

$$\leq \|\nabla f - g\|_2^2. \quad (41)$$

In Equation 40, we can apply the Pythagorean Theorem  $\|a\|_2^2 + \|b\|_2^2 = \|a + b\|_2^2$  for two orthogonal vectors  $a, b$  since  $P_U(\nabla f) - g \in U$  as both  $P_U(\nabla f), g \in U$  and  $\nabla f - P_U(\nabla f) \in U^\perp$  per definition of the orthogonal projection and thus  $P_U(\nabla f) - g$  and  $\nabla f - P_U(\nabla f)$  are orthogonal. Finally, since  $\|\cdot\|_2 \geq 0$  and  $x^2$  monotonically increasing for  $x \geq 0$ , it follows that  $\|\nabla f - P_U(\nabla f)\|_2 \leq \|\nabla f - g\|_2$ . Thus,  $P_U(\nabla f)$  minimizes  $\|\nabla f - g\|_2$  for  $g \in U$ , making it the most accurate approximation of  $\nabla f$  in  $U$ . □

## A.2 Detailed Derivation of the Forward Gradient Time Complexity

Evaluating  $f$  and computing  $k$  forward-mode AD passes requires

$$\omega \cdot \text{ops}(f) \text{ with } \omega \leq 1 + 1.5k \quad (42)$$

time, where  $\text{ops}(f)$  is the time required for evaluating  $f$ , i.e., inference (Griewank and Walther, 2008). The time complexity is thus  $\mathcal{O}(k \cdot \text{ops}(f))$ .

Computing the single-tangent forward gradient  $g_v$  performs one forward-mode AD pass ( $k = 1$ ) and multiplies the resulting scalar directional derivative  $\nabla f \cdot v$  with the  $n$ -dimensional tangent  $v$ . This results in a complexity of

$$T_{g_v} \in \mathcal{O}(\text{ops}(f) + n) = \mathcal{O}(\text{ops}(f)), \quad (43)$$

which is dominated by  $\text{ops}(f)$  since  $f$  needs to at least consider each of its  $n$  parameters once, and thus  $\mathcal{O}(n) \subseteq \mathcal{O}(\text{ops}(f))$ . We use  $T_g$  to indicate the time required to compute an approximate gradient  $g$ .

The multi-tangent forward gradients  $g_V^+$  require  $k$  forward-mode AD passes with time complexity  $\mathcal{O}(k \cdot \text{ops}(f))$  to compute a vector  $V^\top \nabla f$  of  $k$  directional derivatives, followed by multiplication with the  $n \times k$  tangent matrix  $V$ . This results in a complexity of

$$T_{g_V^+} \in \mathcal{O}(k \cdot \text{ops}(f) + nk) = \mathcal{O}(k \cdot \text{ops}(f)). \quad (44)$$

Using  $\overline{g_V}$  instead of  $g_V^+$  corresponds to multiplying  $g_V^+$  by the scalar  $\frac{1}{k}$ , which is again dominated by the other terms, and thus

$$T_{\overline{g_V}} \in \mathcal{O}(k \cdot \text{ops}(f)). \quad (45)$$

Correcting the forward gradient with orthogonal projection  $P_U(\nabla f)$  requires the additional computation of, and multiplication by, the  $k \times k$  inverse Gram matrix  $(\mathbf{V}^\top \mathbf{V})^{-1}$ . This results in an overhead of  $\mathcal{O}(k^2 n)$  for the Gram matrix  $\mathbf{V}^\top \mathbf{V}$ ,  $\mathcal{O}(k^3)$  for its inversion, and  $\mathcal{O}(k^3)$  for the multiplication with the vector of directional derivatives  $\mathbf{V}^\top \nabla f$ . Since  $P_U(\nabla f)$  is exact for all  $k \geq n$ , there is no advantage to using  $k > n$ , and we can thus assume  $k \leq n$ . This simplifies the overhead to

$$T_{P_U(\nabla f)} - T_{g_V^+} \in \mathcal{O}(k^2 n) + \mathcal{O}(k^3) + \mathcal{O}(k^3) = \mathcal{O}(k^2 n), \quad (46)$$

resulting in an overall complexity of

$$T_{P_U(\nabla f)} \in \mathcal{O}(k \cdot \text{ops}(f) + k^2 n). \quad (47)$$

For small, constant  $k$  as used for most of our experiments, this overhead is negligible compared to the forward-mode AD passes in  $\mathcal{O}(k \cdot \text{ops}(f))$ . However, it must be considered for arbitrarily large  $k$ , where it can limit scalability.



## B EXPERIMENTAL METHODS

### B.1 Hyperparameter Optimization

Due to the vastly different gradient magnitudes illustrated in Section 4.1, which depend on the dimensionality  $n$ , the number of tangents  $k$ , and the aggregation approach, we performed an extensive hyperparameter search to obtain a suitable learning rate for each approach and task. Specifically, we apply Propulate (Taubert et al., 2023), a Python package for parallel hyperparameter optimization using an asynchronous evolutionary algorithm, to search the logarithmic space  $[1 \times 10^{-6}, 1]$ . We use the single-island model with default values for propagator and propulator, population size 8, 25 generations, and 4 parallel workers. To limit the computation time, we employ two early stopping mechanisms to abort unpromising runs early. A run-local early stopping mechanism terminates the run if there is no improvement over  $p$  steps, with  $p = 100$  steps for optimizing closed-form functions and  $p = 10$  epochs for training neural networks. Additionally, runs unlikely to improve upon previous runs are stopped using a modified version of Propulate’s surrogate model. The surrogate model aborts a run if its difference from the global optimum (zero in the case of neural network loss) is more than twice that of the best run so far for more than 5 % of total steps/epochs. For ResNet18 and VisionTransformer, we further limit the number of epochs for the learning rate search to 50. After the optimization, we select the best learning rate; if multiple learning rates obtain the same results, we select the one closest to their average. The final learning rates used in our experiments are listed in Tables 2 to 4; to aid reproducibility, they are also included as .csv files in the source code repository.

Table 2: The learning rates used to train neural networks in Sections 4.4 and 4.5.

|                  | $k$ | <b>FC, <math>w = 256</math></b> | <b>FC, <math>w = 1024</math></b> | <b>FC, <math>w = 4096</math></b> | <b>ResNet18</b>      |                      | <b>VisionTransformer</b> |                      |
|------------------|-----|---------------------------------|----------------------------------|----------------------------------|----------------------|----------------------|--------------------------|----------------------|
|                  |     | <b>MNIST</b>                    | <b>MNIST</b>                     | <b>MNIST</b>                     | <b>MNIST</b>         | <b>CIFAR10</b>       | <b>MNIST</b>             | <b>CIFAR10</b>       |
| $\nabla f$       | –   | $2.6 \times 10^{-2}$            | $3.3 \times 10^{-2}$             | $3.9 \times 10^{-2}$             | $1.1 \times 10^{-1}$ | $9.9 \times 10^{-4}$ | $2.0 \times 10^{-1}$     | $2.3 \times 10^{-3}$ |
| $g_v$            | 1   | $5.6 \times 10^{-4}$            | $1.6 \times 10^{-4}$             | $7.1 \times 10^{-5}$             | $7.1 \times 10^{-5}$ | $3.4 \times 10^{-4}$ | $2.1 \times 10^{-5}$     | $5.0 \times 10^{-5}$ |
| $\overline{g_V}$ | 2   | $8.5 \times 10^{-4}$            | $2.2 \times 10^{-4}$             | $1.3 \times 10^{-4}$             | $2.8 \times 10^{-4}$ | $7.2 \times 10^{-4}$ | $3.4 \times 10^{-5}$     | $6.6 \times 10^{-5}$ |
|                  | 4   | $8.2 \times 10^{-4}$            | $6.0 \times 10^{-4}$             | $1.8 \times 10^{-4}$             | $2.1 \times 10^{-4}$ | $1.3 \times 10^{-3}$ | $3.6 \times 10^{-5}$     | $7.6 \times 10^{-5}$ |
|                  | 16  | $1.4 \times 10^{-3}$            | $2.7 \times 10^{-3}$             | $5.0 \times 10^{-4}$             | $4.3 \times 10^{-4}$ | $2.5 \times 10^{-3}$ | $7.1 \times 10^{-5}$     | $1.9 \times 10^{-4}$ |
| $P_U$            | 2   | $2.1 \times 10^{-1}$            | $2.3 \times 10^{-1}$             | $4.6 \times 10^{-1}$             | $5.1 \times 10^{-1}$ | $4.9 \times 10^{-1}$ | $4.9 \times 10^{-1}$     | $1.0 \times 10^0$    |
|                  | 4   | $1.2 \times 10^{-1}$            | $2.0 \times 10^{-1}$             | $3.5 \times 10^{-1}$             | $5.1 \times 10^{-1}$ | $4.9 \times 10^{-1}$ | $4.9 \times 10^{-1}$     | $1.0 \times 10^0$    |
|                  | 16  | $4.2 \times 10^{-2}$            | $1.3 \times 10^{-1}$             | $2.5 \times 10^{-1}$             | $1.2 \times 10^{-1}$ | $4.9 \times 10^{-1}$ | $4.9 \times 10^{-1}$     | $4.9 \times 10^{-1}$ |

Table 3: The learning rates used to optimize *Styblinski-Tang* with  $\overline{g_V}$  for different angles between the random tangents in Section 4.3.

| $k$ | 15°                  | 30°                  | 45°                  | 60°                  | 75°                  | 90°                  |
|-----|----------------------|----------------------|----------------------|----------------------|----------------------|----------------------|
| 16  | $2.6 \times 10^{-2}$ | $3.6 \times 10^{-2}$ | $2.6 \times 10^{-2}$ | $3.5 \times 10^{-2}$ | $3.5 \times 10^{-2}$ | $3.5 \times 10^{-2}$ |
| 64  | $2.6 \times 10^{-2}$ | $3.5 \times 10^{-2}$ | $3.5 \times 10^{-2}$ | $3.5 \times 10^{-2}$ | $3.5 \times 10^{-2}$ | $3.5 \times 10^{-2}$ |



## B.2 Experimental Details

In this section, we give all the necessary details to reproduce our results from Section 4. For the approximation quality in Sections 4.1 and 4.3, we assume a fixed gradient of  $(1, \dots, 1)^\top$ , this corresponds to the function  $f(x) = \sum_{i=1}^n x_i$ . We then compute the different forward gradients, sampling the tangent(s) for 1000 different random seeds, measuring their cosine similarity and norm compared to the true gradient  $\nabla f$ , and averaging the result over the random seeds. In Sections 4.2 and 4.3, we optimize three functions: *Sphere*  $f_{\text{SP}}$ , *Rosenbrock*  $f_{\text{RB}}$  (Rosenbrock, 1960), and *Styblinski-Tang*  $f_{\text{ST}}$  (Styblinski and Tang, 1990) with

$$f_{\text{SP}} = \sum_{i=1}^n x_i \quad (48)$$

$$f_{\text{RB}} = \sum_{i=1}^{n-1} 100(x_{i+1} - x_i^2) + (1 - x_i)^2 \quad (49)$$

$$f_{\text{ST}} = \frac{1}{2} \sum_{i=1}^n x_i^4 - 16x_i^2 + 5x_i. \quad (50)$$

We start at the initial values  $x_{\text{SP}}^0 = (-1, \dots, -1)^\top$ ,  $x_{\text{RB}}^0 = (-1, 0, \dots, 0)^\top$ ,  $x_{\text{ST}}^0 = (0, \dots, 0)^\top$  and update  $x$  in each step via gradient descent according to the (approximate) gradient, using the learning rates specified in Appendix B.1. The initial value is independent of the random seed; the random seed affects only the random sampling of tangents for the forward gradients. We perform up to 1000 update steps for *Sphere* and *Styblinski-Tang* and 25 000 for *Rosenbrock*, with early stopping after 50 steps without improvement. We report the best value achieved during the optimization as average over five random seeds (0 to 4).

In Sections 4.4 and 4.5, we train different neural networks on MNIST (Lecun et al., 1998) and CIFAR10 (Krizhevsky, 2009). For both tasks, we use the usual 10 000 sample test set and split another 10 000 samples from the training set to be used for validation, both during the learning rate search and for early stopping during training. We normalize the images but apply no other data augmentation. All networks are trained for 200 epochs with early stopping after ten epochs without improvement, using a batch size of 64 for MNIST and 128 for CIFAR10. We use SGD without momentum or weight decay and with a constant learning rate, as given in Appendix B.1.

In Section 4.4, we train fully-connected networks with hidden layer width  $w$  following the architecture

$$\text{FC}w\text{-ReLU-FC}w\text{-ReLU-FC10},$$

where FC $w$  is a fully-connected layer with  $w$  output neurons. We evaluate three different layer widths:  $w = 256$ ,  $w = 1024$ , and  $w = 4096$ . The input image is flattened to a one-dimensional vector before it is passed to the first layer. In Section 4.5, we train a ResNet18 (He et al., 2016) and a small vision transformer (Dosovitskiy et al., 2021) with six layers, four heads, 256 hidden dimensions, and 512 MLP dimensions.

For the forward gradients, we use activity perturbation instead of weight perturbation, which has been found to reduce the variance of forward gradients in neural networks since the activations are typically of lower dimension than the weights (Ren et al., 2023). That is, we compute the forward gradients with respect to the output activation of a layer and determine the gradients of the layer-internal weights analytically based on the activation gradient. For this, we use the following definition of layers: for the fully-connected network, each FC-layer is considered together with its subsequent activation; for the residual network, each of the four residual blocks is considered as a layer, with the processing both before and after the residual blocks grouped into another layer; finally, for the vision transformer, each encoder layer is considered as layer, with the input and output processing merged into the first and last layers, respectively. At the moment, we simulate the forward gradient computation via backpropagation, i.e., explicitly computing  $\nabla f$  and multiplying it with the tangents  $v$ , instead of computing actual forward-mode AD passes. This allows us to quickly test even large numbers of tangents and take advantage of the extensive tooling and highly efficient implementation available for backpropagation. While this is equivalent in terms of the computed forward gradient, it differs in the time complexity and makes runtime measurements of the forward gradient less meaningful.

## C ADDITIONAL RESULTS

In Section 4.2, we find that increasing  $k$  consistently improves the optimization performance of the forward gradient, with one exception: optimizing the *Rosenbrock* function for  $n = 4$  and  $n = 8$ . Here, we give some more insights on this specific task. Table 5 shows the best result for each approach, both per individual random seed and as the mean over all random seeds. The mean over all seeds corresponds to the values illustrated in Figure 4. The results are shaded in blue to highlight worse runs in darker colors.

For  $n = 4$ , all but one run successfully minimize the function. Only  $\overline{g_V}$ ,  $k = 4$  for random seed 3 cannot improve further than 3.70, increasing the average for  $\overline{g_V}$ ,  $k = 4$  to 0.74. Increasing the dimension to  $n = 8$  makes the optimization more challenging and increases the number of unsuccessful runs. We observe that all approaches except the exact gradients  $\nabla f$  and  $P_U$ ,  $k = 16 > 8 = n$  result in at least one unsuccessful run, with  $P_U$  being more robust than  $\overline{g_V}$ . Overall, we note that except for  $\overline{g_V}$ ,  $k = 16$ ,  $n = 8$ , all runs either come close to the optimum of zero or remain far from the optimum around a value of four. The mean over all seeds is more diverse and depends primarily on how many of the five seeds successfully minimize the function. When taking the learning rate  $\eta$  into account, we find that increasing  $k$  tends to increase the best learning rate found for  $\overline{g_V}$ . However, due to the complexity of *Rosenbrock*, a few missteps can quickly lead to divergence or suboptimal local minima. This increase in learning rate can thus make multi-tangent forward gradients more sensitive to the random seed, as it makes potential missteps more impactful.

Table 5: Detailed results per random seed for *Rosenbrock*  $n = 4$  and  $n = 8$ . The mean over all random seeds (last column) corresponds to the values illustrated in Figure 4. The global minimum of the *Rosenbrock* function is zero; values are shaded in blue, using darker colors for larger (= worse) values. Due to the complexity of the *Rosenbrock* function and the increased learning rate of multi-tangent forward gradients, small  $k > 1$  can be more sensitive to the random seed.

|         | $k$              | LR $\eta$ | Best Value           |        |        |        |        | Mean |
|---------|------------------|-----------|----------------------|--------|--------|--------|--------|------|
|         |                  |           | Seed 0               | Seed 1 | Seed 2 | Seed 3 | Seed 4 |      |
| $n = 4$ | $\nabla f$       | —         | $1.2 \times 10^{-3}$ | 0.00   | 0.00   | 0.00   | 0.00   | 0.00 |
|         | $g_v$            | 1         | $4.7 \times 10^{-4}$ | 0.00   | 0.00   | 0.00   | 0.00   | 0.00 |
|         | $\overline{g_V}$ | 2         | $7.6 \times 10^{-4}$ | 0.00   | 0.00   | 0.00   | 0.00   | 0.00 |
|         |                  | 4         | $9.9 \times 10^{-4}$ | 0.00   | 0.00   | 0.00   | 3.70   | 0.74 |
|         |                  | 16        | $1.3 \times 10^{-3}$ | 0.00   | 0.00   | 0.00   | 0.00   | 0.00 |
|         | $P_U$            | 2         | $1.9 \times 10^{-3}$ | 0.00   | 0.00   | 0.00   | 0.00   | 0.00 |
|         |                  | 4         | $1.3 \times 10^{-3}$ | 0.00   | 0.00   | 0.00   | 0.00   | 0.00 |
|         |                  | 16        | $1.2 \times 10^{-3}$ | 0.00   | 0.00   | 0.00   | 0.00   | 0.00 |
| $n = 8$ | $\nabla f$       | —         | $1.1 \times 10^{-3}$ | 0.00   | 0.00   | 0.00   | 0.00   | 0.00 |
|         | $g_v$            | 1         | $2.3 \times 10^{-4}$ | 0.00   | 3.99   | 0.00   | 0.00   | 0.80 |
|         | $\overline{g_V}$ | 2         | $4.2 \times 10^{-4}$ | 3.99   | 0.00   | 0.00   | 3.99   | 1.59 |
|         |                  | 4         | $6.0 \times 10^{-4}$ | 3.99   | 0.00   | 0.00   | 3.99   | 2.39 |
|         |                  | 16        | $1.3 \times 10^{-3}$ | 0.13   | 0.29   | 0.17   | 0.07   | 0.99 |
|         | $P_U$            | 2         | $1.9 \times 10^{-3}$ | 3.99   | 0.00   | 0.00   | 3.99   | 1.59 |
|         |                  | 4         | $1.8 \times 10^{-3}$ | 0.00   | 0.00   | 0.00   | 3.99   | 0.80 |
|         |                  | 16        | $1.1 \times 10^{-3}$ | 0.00   | 0.00   | 0.00   | 0.00   | 0.00 |